Infrared Physics & Technology 76 (2016) 408–414

Contents lists available at ScienceDirect

Infrared Physics & Technology

journal homepage: www.elsevier.com/locate/infrared

Gaussian mixture model-based gradient field reconstruction for infrared image detail enhancement and denoising

Fan Zhao [a,b], Jian Zhao [a,*], Wenda Zhao [a,b], Feng Qu [a]

[a] Changchun Institute of Optics, Fine Mechanics and Physics, Chinese Academy of Sciences, Changchun 130033, China
[b] University of Chinese Academy of Sciences, Beijing 100049, China

ARTICLE INFO

Article history:
Received 25 May 2015
Revised 24 March 2016
Accepted 30 March 2016
Available online 31 March 2016

Keywords:
Infrared image detail enhancement and denoising
Gaussian mixture model
Gradient field reconstruction
Anisotropic diffusion constraint

ABSTRACT

Infrared images are characterized by low signal-to-noise ratio and low contrast. Therefore, the edge details are easily immerged in the background and noise, making it much difficult to achieve infrared image edge detail enhancement and denoising. This article proposes a novel method of Gaussian mixture model-based gradient field reconstruction, which enhances image edge details while suppressing noise. First, by analyzing the gradient histogram of noisy infrared image, Gaussian mixture model is adopted to simulate the distribution of the gradient histogram, and divides the image information into three parts corresponding to faint details, noise and the edges of clear targets, respectively. Then, the piecewise function is constructed based on the characteristics of the image to increase gradients of faint details and suppress gradients of noise. Finally, anisotropic diffusion constraint is added while visualizing enhanced image from the transformed gradient field to further suppress noise. The experimental results show that the method possesses unique advantage of effectively enhancing infrared image edge details and suppressing noise as well, compared with the existing methods. In addition, it can be used to effectively enhance other types of images such as the visible and medical images.

© 2016 Elsevier B.V. All rights reserved.

1. Introduction

Image enhancement technology plays an important role in the whole image processing [1,2] and has been applied to many areas, such as remote sensing image, medical image [3,4], stereo image and retinex image [5–7]. Generally, infrared images have small signal to noise ratio (SNR) and low contrast, therefore the edge detail is easily immerged in the background and noise, making it difficult for target detection and tracking [8,9]. In order to provide high-quality infrared image information for applications, it is necessary to enhance edge details and denoising. For noisy infrared images, edge details can be enhanced by traditional methods, but noise increases simultaneously. This is because the weak details are submerged in the noise. For example, the classic histogram equalization [10,11] algorithms produce an unsatisfactory result when they enhance noisy infrared images. Therefore, it is a challenge and necessary for infrared image detail enhancement and denoising.

Many improvements have been proposed such as platform histogram equalization [12,13] and double platform histogram equalization [8,14]. They enhance the image details and suppress noise by setting one or two platform thresholds. But it is difficult to properly choose the threshold values. Another method is based on histogram specification [15]. Wang et al. find the guiding function by maximizing the entropy, under the constraints that the mean brightness. Other typical methods for infrared image enhancement and denoising are based on wavelet transform [16–18]. Zhou et al. use a stationary multi-wavelet transform method to remove noise [16]. Wang et al. extract signal from noise according to phases and modulus maxima of dyadic wavelet transform coefficients of the infrared image, and the wavelet coefficients belonging to noise are eliminated at each scale [17]. Ni et al. combine wavelet modulus and local singularity into a joint conditional model to build an elementary edge map, then the edge map with geometric consistency is updated to reduce noise in infrared images while enhancing edges [18]. For most infrared images, the above wavelet-based methods can suppress noise and enhance edge details. However, the complexity of the wavelet-based methods limits their application in engineering.

Gradients of the image play an important role, where the gradients are big and image edge details are clear. Wang et al. uses the image gradient to adaptively determine the scale and orientation of anisotropic Gaussian filter, and this suppresses noise while preserving the edge details [19]. Zuo et al. enhance image texture and denoising by enforcing the gradient histogram of the denoised image to be close to a reference gradient histogram of the original image [20]. In [21], Zhao et al. enhance the edge details of the

* Corresponding author.
E-mail address: zhaojian6789@126.com (J. Zhao).

http://dx.doi.org/10.1016/j.infrared.2016.03.022
1350-4495/© 2016 Elsevier B.V. All rights reserved.

infrared image by constructing a Gaussian function to expand the gradient histogram. For noise-free images, it can achieve good results. However, for noise images, it enhances image details while increasing noise. In this paper, Gaussian mixture model-based gradient field reconstruction for infrared image detail enhancement and denoising is proposed. Gaussian mixture model is used to simulate the distribution of the gradient histogram, dividing the gradients into three ranges corresponding to faint details, noise and the edges of clear targets and background, respectively. Then, the piecewise function is constructed to increase gradients of faint details and suppress gradients of noise, which will be introduced in part A of Section 2. In order to further suppress noise, anisotropic diffusion constraint is added while reconstructing enhanced image from the converted gradient field, which will be introduced in part B of Section 2. The effectiveness of the proposed method will be discussed in Section 3, followed by a brief conclusion.

2. Proposed method

For a pixel $i(x_1,x_2)\subset\Omega$ in the infrared image $\mathbf{I}$, where $(x_1,x_2)\subset\Omega=[0,L-1]\times[0,W-1]$, if the gradient is $\nabla i(x,y)$, then gradient magnitude value $|\nabla i(x,y)|$ and gradient direction θ are defined as:

$$\nabla i(x,y)=\left[\frac{\partial i(x,y)}{\partial x},\frac{\partial i(x,y)}{\partial y}\right] \tag{1}$$

$$|\nabla i(x,y)|=\sqrt{\left|\frac{\partial i(x,y)}{\partial x}\right|^2+\left|\frac{\partial i(x,y)}{\partial y}\right|^2} \tag{2}$$

$$\theta=\arctan\left[\left|\frac{\partial i(x,y)}{\partial y}\right|\Big/\left|\frac{\partial i(x,y)}{\partial x}\right|\right] \tag{3}$$

where ∇ represents the gradient operator. In order to obtain the gradient histogram of the infrared image, we calculate the histogram of the image using the gradient values instead of the gray level values. For example, the gradient magnitude map and gradient histogram of the infrared image are shown in Fig. 1.

As can be seen from Fig. 1(a), faint details of noisy infrared image are fuzzy, such as the windows of the ship. And the gradients of the faint details are small, as shown in Fig. 1(b). Fig. 1(c) is the gradient histogram of the noisy infrared image. It consists of three ranges: small gradient range corresponding to faint details, the transition range of the small gradients to large gradients mainly containing noise, and large gradient range corresponding to clear object edges. What we will do is using Gaussian mixture model to simulate the distribution of the gradient histogram, dividing the gradient histogram into the above three gradient ranges. Then, the piecewise function is constructed based on the characteristics of the correspondent gradient range to enhance the faint details while suppressing noise.

A. Gaussian mixture model-based gradient field enhancement

The gradient distribution $p^g(i^g)$, where $i^g=|\nabla i|$ is the gradient value of the pixel i, of the input image $\mathbf{I}$ can be modeled as a density function composed of a linear combination of functions [22]:

$$p^g(i^g)=\sum_{n=1}^{N}P^g(w_n)p^g(i^g|w_n) \tag{4}$$

where $P^g(w_n)$ is the prior probability of the Gaussian component w_n and $p^g(i^g|w_n)$ is the nth component density. The component density function is defined as:

$$p^g(i^g|w_n)=\frac{1}{\sqrt{2\pi\sigma_{w_n}^2}}\exp\left(-\frac{(i^g-\mu_{w_n})^2}{2\sigma_{w_n}^2}\right) \tag{5}$$

where μ_{w_n} and $\sigma_{w_n}^2$ are the mean and the variance of gradients of the nth component, respectively.

A Gaussian mixture model is completely determined by the parameters $\theta=\{P(w_n),\mu_{w_n},\sigma_{w_n}^2\}_{n=1}^{N}$. In order to estimate θ, maximum-likelihood-estimation techniques are widely used, such as the expectation maximization (EM) algorithm [23]. Assuming the gradients $\nabla\mathbf{I}=\{i_1^g,i_2^g,\ldots,i_{L\times W}^g\}$ are independent, the likelihood of gradients $\nabla\mathbf{I}$ is computed as follows:

$$\zeta(\nabla\mathbf{I};\theta)=\prod_{\forall k}p(i_k^g;\theta) \tag{6}$$

In order to easily analyze equation (6), the log-likelihood is used:

$$L(\nabla\mathbf{I};\theta)=\log\zeta(\nabla\mathbf{I};\theta)=\sum_{\forall k}p(i_k^g;\theta) \tag{7}$$

The goal of the estimation is to find $\hat{\theta}$ which maximizes the log-likelihood, which is expressed as:

$$\hat{\theta}=\arg\max_{\theta}L(\nabla\mathbf{I};\theta) \tag{8}$$

The EM is a local optimization algorithm, and it is sensitive to initial value [23]. Here, we use its improved variant: the Figueiredo–Jain (FJ) algorithm [24], which overcomes the major shortcomings of the EM algorithm, for parameter estimation. It can automatically remove the data that is not supported in the process of estimation, which avoids the generation of the variation element. In addition, it sets an element for each sample, and allows an arbitrary initial value of the EM algorithm as the initial guess value of the element. The initial guess value can be distributed into the whole space by continuous sampling. The detailed description of the FJ algorithm can be found in Figueiredo and Jain's paper [24]. Fig. 2 illustrates the Gaussian mixture model distribution of the gradient histogram of Fig. 1(c).

As is shown in Fig. 2(a), the gradient histogram is modeled using three Gaussian components, i.e., $N=3$. The close match between the gradient histogram (shown as blue line) and the

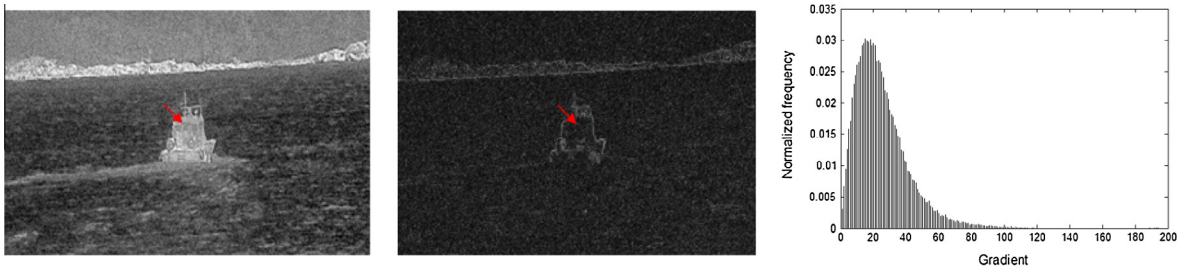

Fig. 1. An example about infrared image and its gradient histogram, (a) noisy infrared image; (b) gradient magnitude map; (c) gradient histogram, where the horizontal axis represents the gradient values and ordinate represents the normalized frequency of the gradient values.

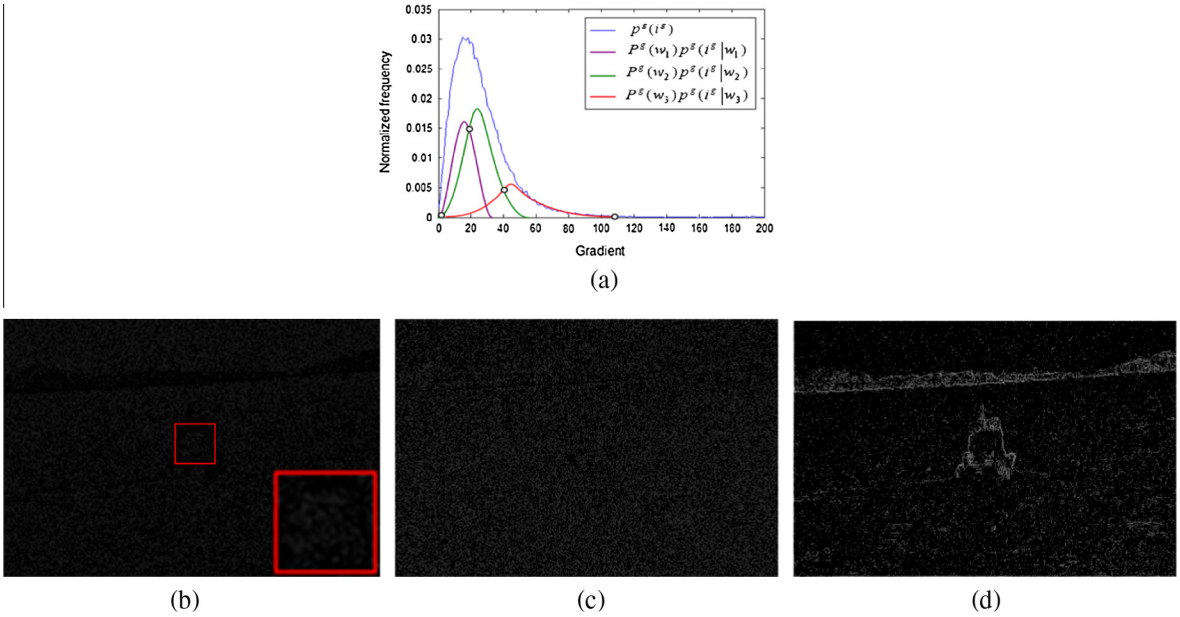

Fig. 2. (a) Gaussian mixture model distribution of the gradient histogram of Fig. 1(c); (b)–(d) gradient maps corresponding to the gradient ranges of [0,19), [19,41) and [41,109], respectively.

Gaussian mixture model fit (shown as purple, green and red lines) is obtained using the FJ algorithm. The intersection points (the calculation method of the intersection points can be found in [25]) denoted by black circles between Gaussian components divide the gradient histogram into three gradient ranges of [0,19), [19,41) and [41,109], respectively. And their gradient maps are shown in Fig. 2(b) and (c). Here, to clearly show the gradient maps of different gradient ranges, other gradients outside corresponding range are expressed as 0. Fig. 2(b) is the gradient map of range ([0,19)), and it contains the gradients of faint details, such as the windows of the ship (enlarged view as shown in the lower right corner denoted by red rectangle). The gradient map of the transition range ([19,41)) of the small gradients to large gradients is shown in Fig. 2(c), and it mainly contains noise. The large gradient range ([41,109]) contains the edges of clear targets and background, as shown in Fig. 2(d).

To enhance the faint details of infrared image while suppressing noise, based on characteristics of different gradient ranges, the piecewise function is constructed to increase the gradients of faint details while suppressing the gradients of the noise, which is expressed as follows.

$$F(i^g)=\begin{cases}1+3\cos\left(\dfrac{i^g-i^g_{w_1^s}}{i^g_{w_1^b}-i^g_{w_1^s}}\cdot\dfrac{\pi}{2}\right) & i^g_{w_1^s}\leqslant i^g<i^g_{w_1^b}\\ \cos\left(\dfrac{i^g-i^g_{w_2^s}}{i^g_{w_2^b}-i^g_{w_2^s}}\cdot\dfrac{\pi}{4}\right) & i^g_{w_2^s}\leqslant i^g<i^g_{w_2^b}\\ \sin\left(\dfrac{\pi}{4}+\dfrac{i^g-i^g_{w_3^s}}{i^g_{w_3^b}-i^g_{w_3^s}}\cdot\dfrac{\pi}{4}\right) & i^g_{w_3^s}\leqslant i^g<i^g_{w_3^b}\end{cases} \tag{9}$$

where $F(\cdot)$ is the piecewise function, and $\left\{i^g_{w_n^s}\right\}_{n=1}^3$ and $\left\{i^g_{w_n^b}\right\}_{n=1}^3$ are the small gradient and big gradient of the intersection points of Gaussian component w_n, respectively. So, the enhanced gradient field is expressed as follows:

$$\mathbf{E}=F(|\nabla u_0|)\cdot\frac{\nabla u_0}{|\nabla u_0|} \tag{10}$$

where $\mathbf{E}$ is the enhanced gradient field, u_0 is the input infrared image, and $\frac{\nabla u_0}{|\nabla u_0|}$ is to keep the direction of image gradient field unchanged. Fig. 3 illustrates the piecewise function and the enhanced gradient magnitude map and images, and the original image is shown in Fig. 1(a).

From Fig. 3(a) can be seen that in the range of [0,19) corresponding to faint details, the function values are greater than 1, and corresponding gradients are increased. In the range of [19,41) mainly containing noise, the function values are smaller than 1, and corresponding gradients are reduced. In the range of [41,109] corresponding to the edges of clear targets and background, the function values are close to 1, and corresponding gradients are preserved. Fig. 3(b) illustrates that the gradients of faint details are increased and gradients of noise are suppressed. Then, the faint details are enhanced while suppressing noise, such as the windows of the ship in Fig. 3(c). However, the reconstructed image still contains a small amount of noise. To further suppress noise, anisotropic diffusion constraint is added while reconstructing enhanced image from the converted gradient field, which will be introduced in section B. And the final enhanced image is shown Fig. 3(d). Edge details of the image are clear and noise is effectively suppressed.

B. Image visualization with anisotropic diffusion constraint

Now we have obtained the enhanced gradient field $\mathbf{E}$. To find a closest image u whose gradients have the least-squared-error to $\mathbf{E}$, we can minimize the following functional:

$$G(u)=\iint_{\Omega}|\nabla u-\mathbf{E}|^2 \tag{11}$$

With the variation method, the Euler–Lagrange equation of (11) is as:

$$\Delta u=div\mathbf{E} \tag{12}$$

Using gradient descent algorithm, we may find:

$$\frac{\partial u}{\partial t}=\Delta u-div\mathbf{E} \tag{13}$$

where Δ is the Laplace operator, and div the divergence operator. The solution u of (13) contains a small amount of noise, as shown in Fig. 3(c). To further suppress noise, anisotropic diffusion constraint is added in the iterations of (13).

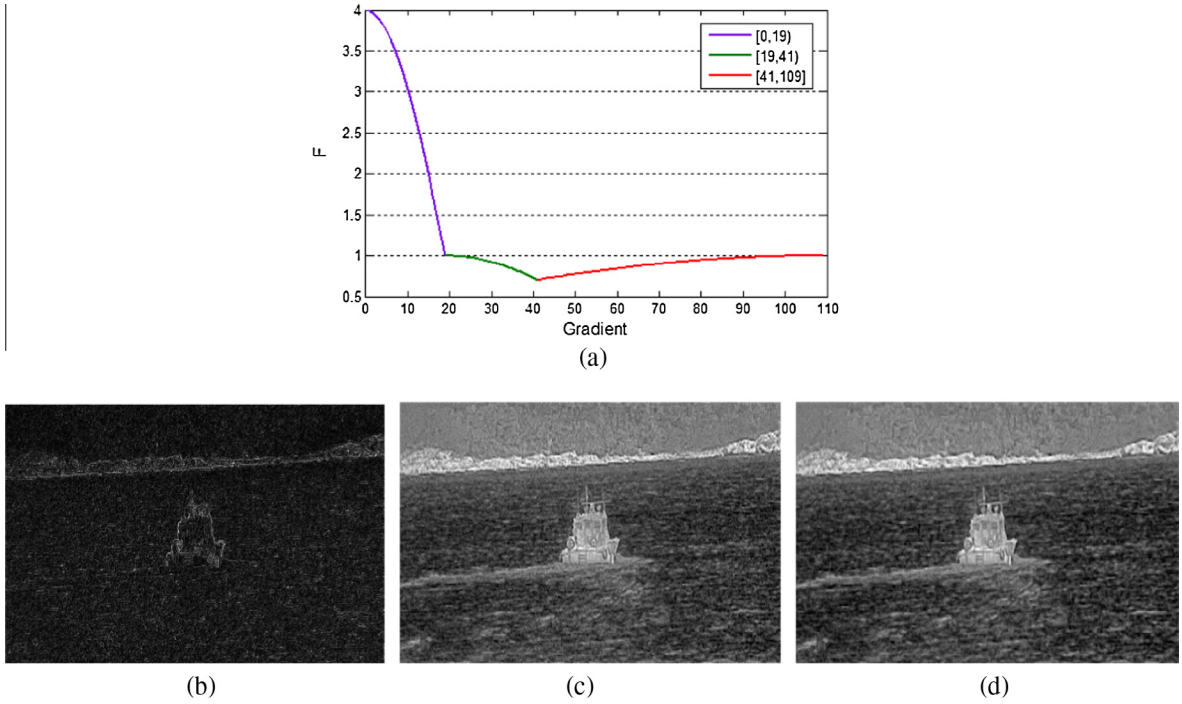

Fig. 3. (a) The piecewise function of Fig. 1(a); (b) enhanced gradient magnitude map; (c) reconstructed image from enhanced gradient field; (d) enhanced image by the proposed method.

Anisotropic diffusion model [26,27] is:

$$\frac{\partial u}{\partial t} = div[g(|\nabla u|)\nabla u] \tag{14}$$

$g(\cdot)$ is diffusion coefficient that controls the behavior of diffusion. Here, $g(\cdot)$ is defined as:

$$g(|\nabla u|) = e^{-\left(\frac{|\nabla u|}{i^g_{w_1^s} + 0.3\cdot\left(i^g_{w_1^b} - i^g_{w_1^s}\right)}\right)} \tag{15}$$

where $i^g_{w_1^b}$ and $i^g_{w_1^s}$ are the big gradient and small gradient of the intersection points of Gaussian component w_1. $i^g_{w_1^s} + 0.3\cdot\left(i^g_{w_1^b} - i^g_{w_1^s}\right)$ is to reduce the spread of diffusion function when gradient values are small, which can preserve the weak edge details. In flat areas, $|\nabla u|$ is small, then the diffusion equation as a low pass filter for smoothing. In the edge region, $|\nabla u|$ is large, then the diffusion behavior of the diffusion equation is not obvious, which preserve the edge information. Comprehensively considering the image edge details enhancement and noise suppression, (13) is redefined as follows:

$$\frac{\partial u}{\partial t} = \Delta u - div\mathbf{E} + \lambda div[g(|\nabla u|)\nabla u] \tag{16}$$

where λ adjusts the proportion of the two parts above. Using finite difference method, the discrete iterative form of (16) is:

$$u^{n+1} = u^n + \tau\{\Delta u^n - div\mathbf{E} + \lambda div[g(|\nabla u^n|)\nabla u^n]\} \tag{17}$$

where n represents the number of iterations, and τ represents the time step.

3. Experimental results

To verify the effectiveness of the method, comparing it with histogram equalization with maximum entropy-based method (HEME) [15], gradient histogram estimation and preservation-based method (GHEP) [20], gradient field specification with Gaussian function-based method (GFSGF) [21], and anisotropic diffusion constraint is added while reconstructing enhanced image from the specification gradient field of [21] (GFSGFADC), we conduct a lot of experiments. The number of iterations n is taken as 20, and λ is taken as 0.25. Here are some experimental results.

Fig. 4(a) is an original noisy infrared image. HEME improves the contrast of the image, but noise is also enhanced, as shown in Fig. 4 (b). GHEP effectively suppresses noise, but weak details are not obviously enhanced, as shown in Fig. 4(c). Fig. 4(d) is the result of GFSGF. Image edge details are significantly enhanced while increasing noisy. Based on GFSGF, we add anisotropic diffusion constraint to suppress noisy, and the result is shown in Fig. 4(e). Noise is partially suppressed, and visual effect is improved. The result of the proposed method is shown in Fig. 4(f). It effectively enhances image edge details and suppresses noise such as the armored car and the woods.

Fig. 5(a) is another noisy infrared image, and the image has unclear texture edges and small SNR. Using HEME, the image contrast is improved, and the details are clearer than Fig. 5(a). GHEP increases SNR of the image and weak details are preserved, as shown in Fig. 5(c). GFSGF and GFSGFADC effectively enhance edge details, but the enhanced images have bigger noise than Fig. 5(a), as shown in Fig. 5(d) and (e). The enhanced image by the proposed method is shown in Fig. 5(f). The texture edges are very clear and noise is effectively suppressed.

Fig. 6(a) is a fuzzy infrared image containing much noise in the dark background. HEME, GFSGF and GFSGFADC respectively enhance image details, but noise is magnified, as shown in Fig. 6(b), (d) and (e). GHEP effectively suppresses noise, and preserves edge detail information, as shown in Fig. 6(c). Compared with the previous four methods, the image enhanced by the proposed method has the clearest edge details and the best visual effect.

To give a quantitative comparison, the measure linear index of fuzziness [28,29] is used in this paper, which is denoted as γ.

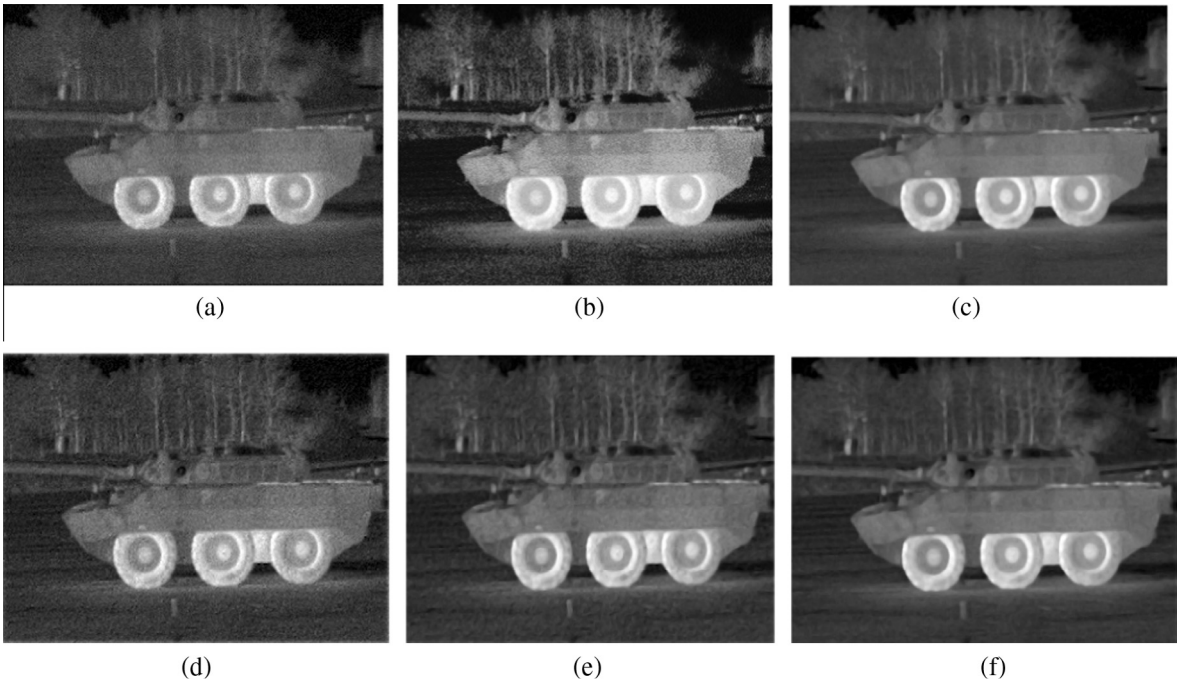

Fig. 4. Experimental results comparison of the armored car. (a) Original noisy infrared image. (b) HEME. (c) GHEP. (d) GFSGF. (e) GFSGFADC. (f) Proposed method.

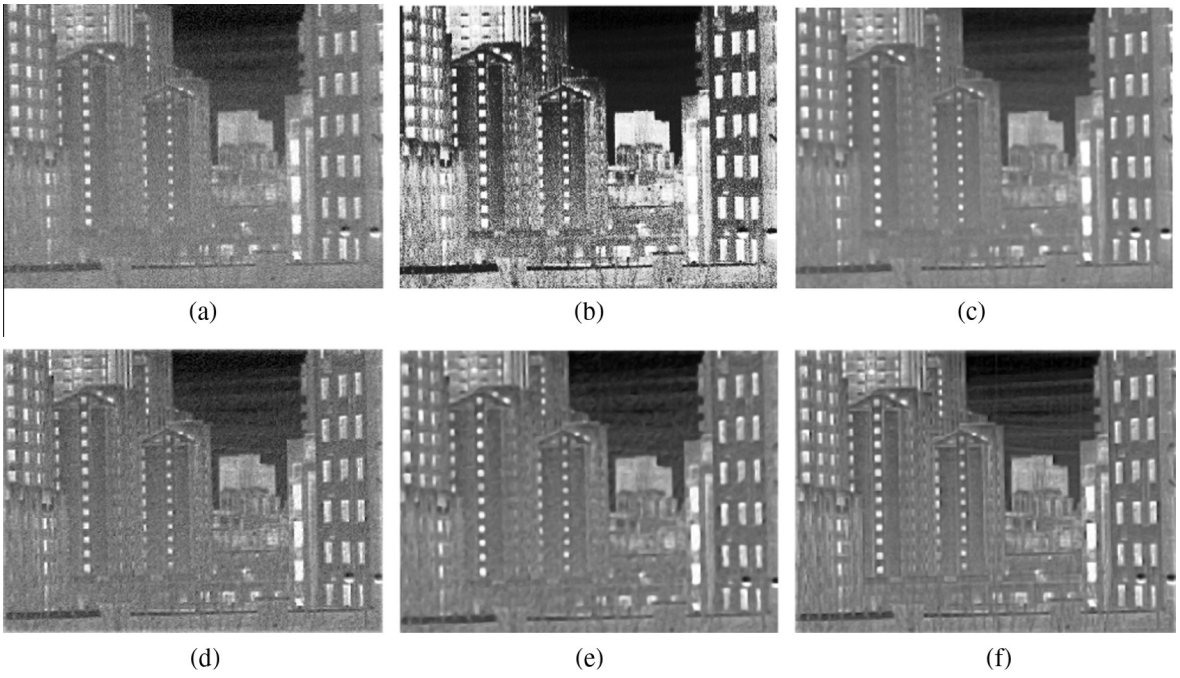

Fig. 5. Experimental results comparison of the buildings. (a) Original noisy infrared image. (b) HEME. (c) GHEP. (d) GFSGF. (e) GFSGFADC. (f) Proposed method.

$$\gamma = \frac{2}{L \cdot W} \sum_{x=1}^{L} \sum_{y=1}^{W} \min \left[\beta_{xy}, (1 - \beta_{xy}) \right] \tag{18}$$

$$\beta_{xy} = \sin \left[\frac{\pi}{2} \cdot \left(1 - \frac{u_{xy}}{u_{\max}} \right) \right] \tag{19}$$

where u_{xy} is the gray value of the pixel (x, y) in the image u, and $u_{\max}$ is the maximum gray value. A small value of γ represents a good enhancement of the image. The values of γ of all the enhanced images obtained by each method are listed in Table 1. Table 1 shows that the values of γ of the enhanced images by the proposed method are smaller than other methods, indicating that our method has a good performance for infrared image detail enhancement and denoising.

The noisy infrared images have been enhanced and denoising by our method, showing a good performance. In addition, the proposed method can also enhance other types of images. Fig. 7 shows the noisy visible and medical images enhanced by the

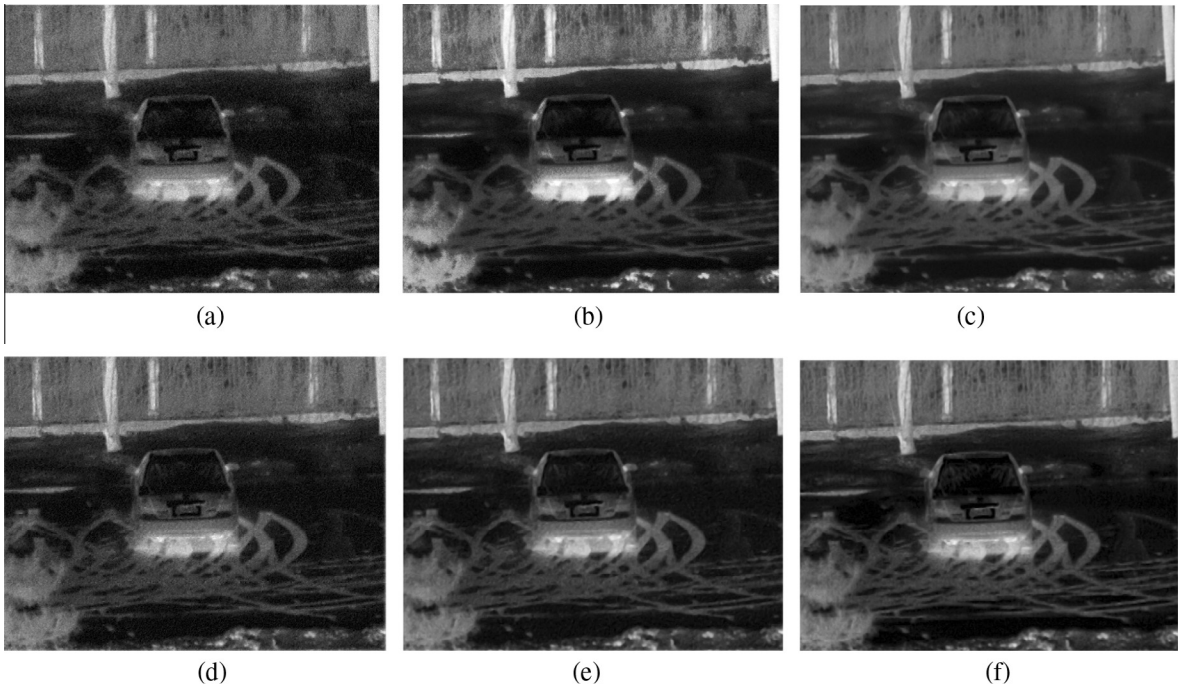

Fig. 6. Experimental results comparison of the car. (a) Original noisy infrared image. (b) HEME. (c) GHEP. (d) GFSGF. (e) GFSGFADC. (f) Proposed method.

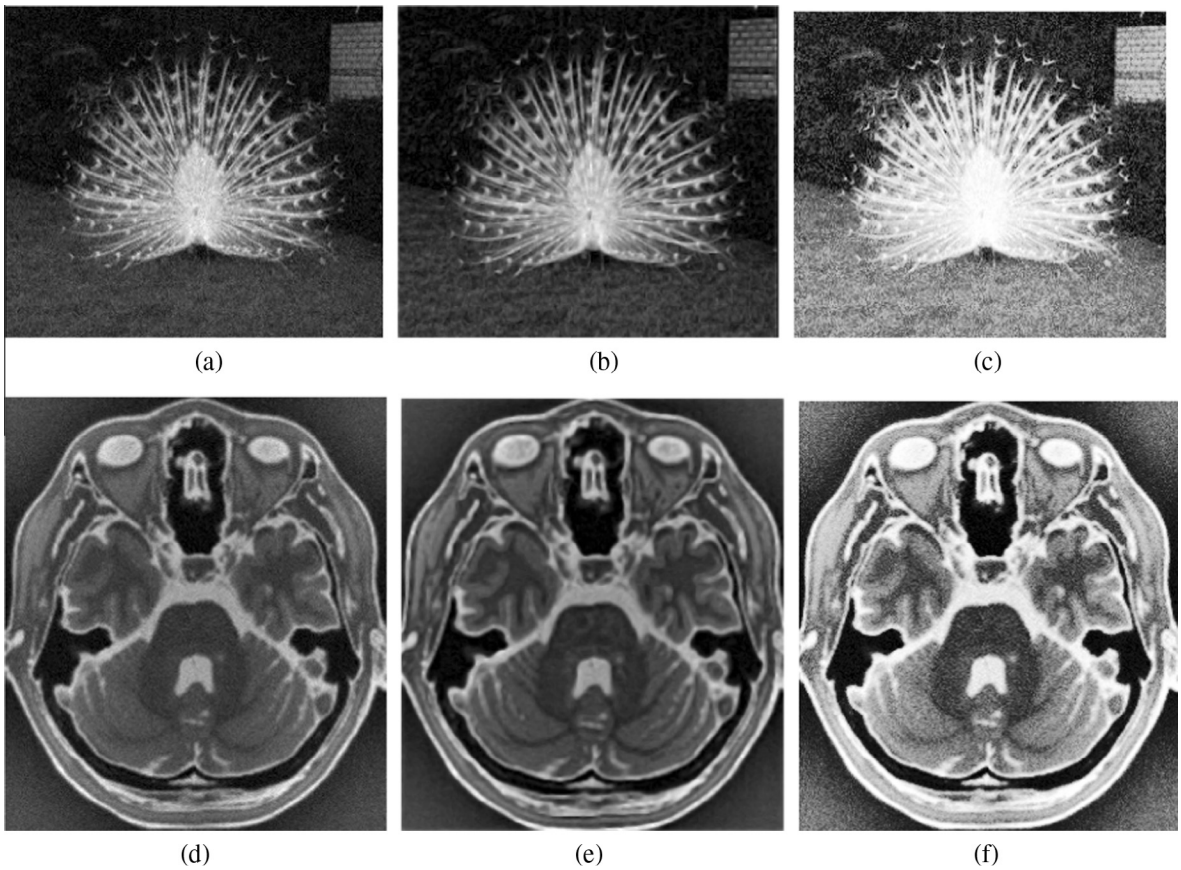

Fig. 7. Experimental results comparison of visible and medical images. (a) Original noisy visible image. (b) Proposed method. (c) HE. (d) Original noisy medical image. (e) Proposed method. (f) HE.

proposed method and the classic histogram equalization (HE) algorithm.

Fig. 7(a) and (d) is the noisy visible and medical images with much noise and fuzzy edge details, respectively. HE improves the image contrast, but the image has been over-enhanced and noise increases, as shown in Fig. 7(c) and (f). After the enhancement by the proposed method, the edge details are clear and noise is effectively suppressed, as shown in Fig. 7(b) and (e).

Table 1
Objective comparison of image enhancement using γ.

	Original image	HEME	GHEP	GFSGF	GFSGFADC	Proposed method
Fig. 4	0.2384	0.2557	0.2383	0.2425	0.2181	0.2148
Fig. 5	0.5380	0.5460	0.5312	0.4980	0.4922	0.4865
Fig. 6	0.1163	0.1312	0.1250	0.1164	0.1120	0.1111

4. Conclusion

In this paper, we present a method of Gaussian mixture model-based gradient field reconstruction for infrared image detail enhancement and denoising. Comparing with other methods, the proposed algorithm has several advantages for infrared image detail enhancement and denoising. Firstly, Gaussian mixture model is adopted to divide the gradients into three ranges corresponding to faint details, noise and the edges of clear targets and background, respectively. Secondly, the piecewise function is constructed to increase gradients of faint details and suppress gradients of noise. Thirdly, anisotropic diffusion constraint is added while reconstructing enhanced image, which can further suppress noise. The experimental results prove that the proposed method performs efficiently. Furthermore, our method can be used to effectively enhance other types of images such as the visible and medical images.

Acknowledgements

The authors would like to thank National Science and Technology Major Project (Grant No. 2013ZX04007021) and Jilin Province Key Science and Technology Project (Grant No. 20140204030GX).

References

[1] A.S. Bar-Noam, N. Farah, S. Shoham, Correction-free remotely scanned two-photon in vivo mouse retinal imaging, Light: Sci. Appl. 5 (2016) e16007.
[2] J. Qin, R.M. Silver, B.M. Barnes, H. Zhou, R.G. Dixson, M.A. Henn, Deep subwavelength nanometric image reconstruction using Fourier domain optical normalization, Light: Sci. Appl. 5 (2016) e16038.
[3] C. Vannahme, M. Dufva, A. Kristensen, High frame rate multiresonance imaging refractometry with distributed feedback dye laser sensor, Light: Sci. Appl. 4 (2015) e269.
[4] D. Qu, Tailoring color emissions from N-doped graphene quantum dots for bioimaging application, Light: Sci. Appl. 4 (2015) e364.
[5] C. Ha, W. Kim, J. Jeong, Remote sensing image enhancement based on singular value decomposition, Opt. Eng. 52 (8) (2013) 083101.
[6] C. Ha, G. Jeon, J. Jeong, Contrast enhancement and noise elimination using singular value decomposition for stereo imaging, Opt. Eng. 51 (9) (2012) 090504.
[7] H.B. Chang, M.K. Ng, W. Wang, T.Y. Zeng, Retinex image enhancement via a learned dictionary, Opt. Eng. 54 (1) (2015) 013107.
[8] K. Liang, Y. Ma, Y. Xue, B. Zhou, R. Wang, A new adaptive contrast enhancement algorithm for infrared images based on double plateaus histogram equalization, Infrared Phys. Technol. 55 (2012) 309–315.
[9] W.D. Zhao, Z.J. Xu, J. Zhao, F. Zhao, X.Z. Han, Variational infrared image enhancement based on adaptive dual-threshold gradient field equalization, Infrared Phys. Technol. 66 (2014) 152–159.
[10] H. Ibrahim, N.S.P. Kong, Brightness preserving dynamic histogram equalization for image contrast enhancement, IEEE Trans. Consum. Electron. 53 (4) (2007) 1752–1758.
[11] S.S. Agaian, B. Silver, K.A. Panetta, Transform coefficient histogram-based image enhancement algorithms using contrast entropy, IEEE Trans. Image Process. 16 (3) (2007) 741–758.
[12] R. Lai, Y.T. Yang, B.J. Wang, H.X. Zhou, A quantitative measure based infrared image enhancement algorithm using plateau histogram, Opt. Commun. 283 (21) (2010) 4283–4288.
[13] C.H. Ooi, N.S.P. Kong, H. Ibrahim, Bi-histogram equalization with a plateau limit for digital image enhancement, IEEE Trans. Consum. Electron. 55 (4) (2009) 2072–2080.
[14] Y.F. Song, X.P. Shao, J. Xu, New enhancement algorithm for infrared image based on double plateaus histogram, Infrared Laser Eng. 37 (2) (2008) 308–331.
[15] C. Wang, Z.F. Ye, Brightness preserving histogram equalization with maximum entropy: a variational perspective, IEEE Trans. Consum. Electron. 51 (4) (2005) 1326–1334.
[16] F.Q. Zhou, X.G. Di, J. Zhou, Method of infrared image denoising based on stationary multiwavelet transform, J. Infrared Millim. Waves 24 (2) (2005) 151–155.
[17] X.W. Wang, S.T. Liu, X.D. Zhou, New algorithm for infrared small target image enhancement based on wavelet transform and human visual properties, J. Syst. Eng. Electron. 17 (2) (2006) 268–273.
[18] C. Ni, Q. Li, L.Z. Xia, A novel method of infrared image denoising and edge enhancement, Signal Process. 88 (2008) 1606–1614.
[19] H.Y. Wang, K. Zhang, Y.J. Li, Anisotropic Gaussian filtering for infrared for infrared image, J. Infrared Millim. Waves 24 (2) (2005) 109–113.
[20] W.M. Zuo, L. Zhang, C.W. Song, D. Zhang, H.J. Gao, Gradient histogram estimation and preservation for texture enhanced image denoising, IEEE Trans. Image Process. 23 (6) (2014) 2459–2472.
[21] W.D. Zhao, Z.J. Xu, J. Zhao, F. Zhao, X.Z. Han, Infrared image detail enhancement based on the gradient field specification, Appl. Opt. 53 (19) (2014) 4141–4149.
[22] D. Reynolds, R. Rose, Robust text-independent speaker identification using Gaussian mixture speaker models, IEEE Trans. Speech Audio Process. 3 (1) (1995) 72–83.
[23] R.O Duda, P.E Hart, D.G Stork, Pattern Classification, second ed., Wiley-Interscience, New York, 2000.
[24] M. Figueiredo, A. Jain, Unsupervised learning of finite mixture models, IEEE Trans. Pattern Anal. Mach. Intell. 24 (3) (2002) 381–396.
[25] T. Celik, T. Tjahjadi, Automatic image equalization and contrast enhancement using gaussian mixture modeling, IEEE Trans. Image Process. 21 (1) (2012) 145–156.
[26] P. Maragos, F. Meyer, A PDE approach to nonlinear image simplification via levelings and reconstruction filters, Canada: 2000 International Conference on Image Processing, vol. 2, 2000, pp. 938–941.
[27] G. Gilboa, Image enhancement and denoising by complex diffusion processes, IEEE Trans. Pattern Anal. Mach. Intell. 26 (8) (2004) 1020–1036.
[28] X.Z. Bai, F.G. Zhou, B.D. Xue, Noise-suppressed image enhancement using multiscale top-hat selection transform through region extraction, Appl. Opt. 51 (3) (2012) 338–347.
[29] R. Lai, Y. Yang, B. Wang, H. Zhou, A quantitative measure based infrared image enhancement algorithm using plateau histogram, Opt. Commun. 283 (2010) 4283–4288.